Remarkable Enhancement of Electrocatalytic Activity by Tuning the Interface of Pd–Au Bimetallic Nanoparticle Tubes

Chun-Hua Cui, Jin-Wen Yu, Hui-Hui Li, Min-Rui Gao, Hai-Wei Liang, and Shu-Hong Yu*

Division of Nanomaterials and Chemistry, Hefei National Laboratory for Physical Sciences at Microscale, Department of Chemistry, University of Science and Technology of China, Hefei 230026, People's Republic of China.

ABSTRACT The interface, which formed in a bimetallic system, is a critical issue to investigate the fundamental mechanism of enhanced catalytic activity. Here, we designed unsupported Pd–Au bimetallic nanoparticle tubes with a tunable interface, which was qualitatively controlled by the proportion of Pd and Au nanoparticles (NPs), to demonstrate the remarkably enhanced effect of Pd and Au NPs in electro-oxidation of ethanol. The results demonstrated that the electrocatalytic activity is highly relative to the interface and has no direct relation with individual metal component in the Pd–Au system. This effect helps us in achieving a fundamental understanding of the relationship between their activity and the interface structure and chemical properties and, consequently, is helpful in designing new catalysts with high performances.

KEYWORDS: interface · Pd–Au nanoparticle tubes · fuel cells · ethanol oxidation · synergistic effect

The enhancement effect of bimetallic catalysts has been one of the most hot and attractive research topics.[1,2] Several explanations for the enhanced activity have been proposed including the size,[3] morphology,[4–6] and interface structure,[7,8] but the relationship between material features of bimetallic catalysts and catalytic activity is still controversial and lacks experimental evidence. Recently, the distinctive catalytic activity of dispersed metal NPs supported on oxides has been extensively studied, and the improved catalytic activity is mainly attributed to the metal/oxide support interface boundary sites.[9–13] Whether the bimetallic NP interface has a role in the promotional effect is still unknown due to technological limitations. First, the bimetallic catalysts should be an unsupported structure to avoid the effect of oxide/carbon support.[2,14–16] Second, to statistically obtain as much interface as possible, the two kinds of metal NPs should be uniformly distributed, and the interface should be effectively exposed as active sites. Third, the interface should be relatively controllable between two metals. However, it is still a challenge to achieve these purposes.

Herein, we report the interface effect of Pd–Au bimetallic catalysts on electrocatalytic activity toward ethanol oxidation through rational synthesis of unsupported Pd–Au bimetallic tubes with controlled Pd/Au NP proportion and uniform particle distribution.

The synthetic route is based on the recently developed one-step non-aqueous solvent electrodeposition by Yu and co-workers.[17,18] The resultant tubular materials demonstrated high surface area and self-supported features and also exhibited high stability and durability during fuel cell operation over particles.[19] The unsupported Pd–Au bimetallic NP heterostructure tubes (BHTs) with 100 to 50 atom % Pd were synthesized by this facile one-step electrodeposition route on an anodic aluminum oxide (AAO) template (see Supporting Information). To avoid the mass transfer limitation of small molecule ethanol, the tube wall thickness should be maintained the same. In the electrochemical synthesis of metal materials, low electrolyte concentration and/or lower potential can benefit the synthesis of the thin tube wall.[20,21] The wall thickness of the tubes should bear the weight and favor the mass transfer of alcohols permeating through the wall. Compared with the synthesis of Pd tubes,[18] the Au tubular structure is more difficult to be synthesized even at lower potential and lower electrolyte concentration due to its high standard potential. So when the Pd ion concentration is kept at 10 mM, the Au ion concentration is increased from 1 to 6 mM, and the applied

* Address correspondence to shyu@ustc.edu.cn.

Received for review March 21, 2011 and accepted April 20, 2011.

Published online April 20, 2011
10.1021/nn2010602

potential is decreased from −1.3 to −1.6 V, as designed in Figure 1. Further evidence is shown in Figure S1 in the Supporting Information.

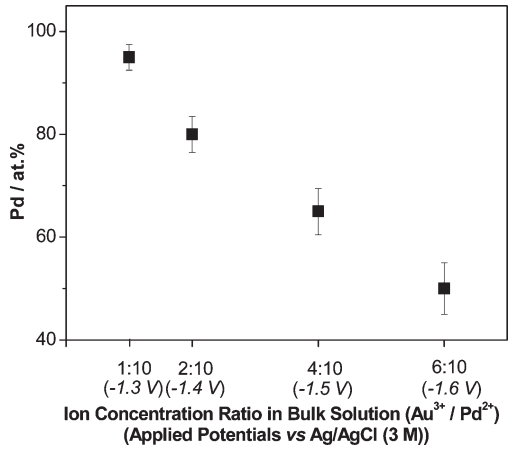

Figure 1. Composition evolution of unsupported Pd−Au BHTs as measured by EDX *versus* metal ion concentration ratio of Au^{3+}/Pd^{2+} in bulk solution and applied potentials *versus* Ag/AgCl (3 M).

The tubular, dispersed, and unsupported Pd−Au BHTs with controlled atom percentage of Pd have been synthesized with several micrometer-sized lengths as measured by scanning electron microscopy (SEM) (Figure 2a,b). The length of the tubes can be controlled by reaction time, and the maximum length is decided by the length of the template channel. A transmission electron microscopy (TEM) image of the Pd−Au BHTs in Figure 2c shows the uniform wall thickness. The average diameter of the Pd−Au BHTs is about 300 nm and corresponds closely to the inner diameter of the template channel. The TEM images indicate that the tube wall is built by many flocky-like spheres, and these spheres consist of tiny nanocrystals (see Supporting Information Figure S2), which is similar to monometallic Pd NP tubes.[18] Moreover, it is clear that the tube is porous, which promotes the mass transfer and effectively exposes the inner and outer surfaces (see Figure S3). The chemical composition including relative atom and mass proportions of as-prepared Pd−Au BHTs was evaluated by energy-dispersive X-ray spectroscopy (EDX) in Figure 3 and further confirmed by inductively coupled plasma mass spectrometry (ICP). The results

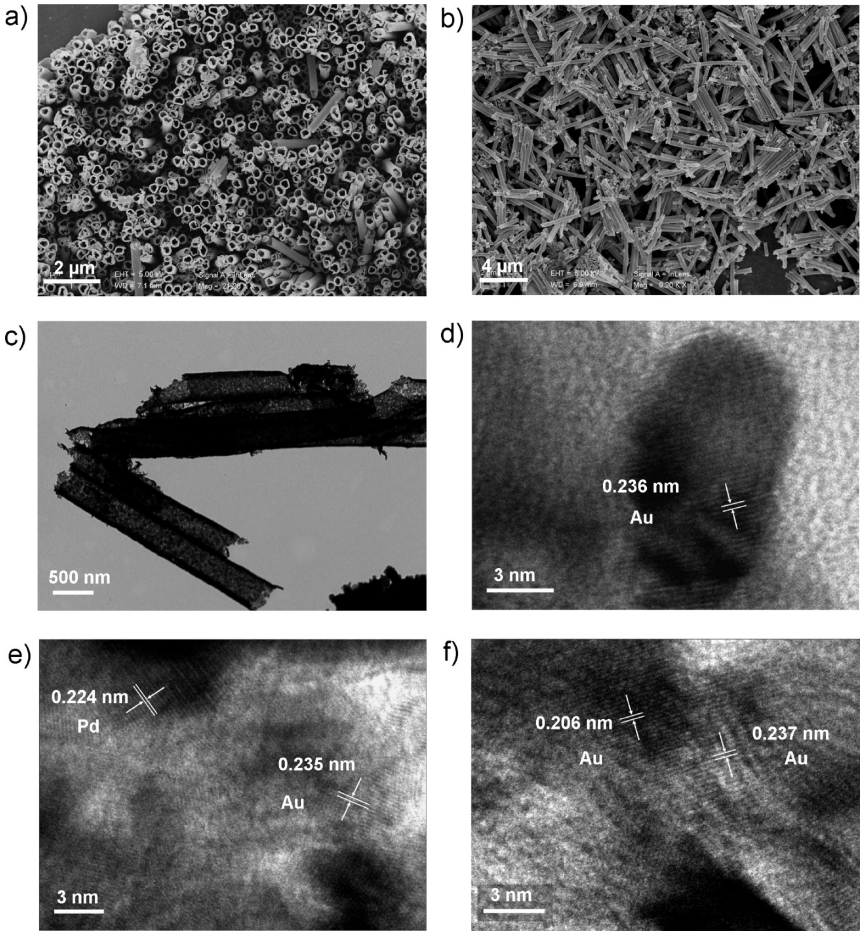

Figure 2. SEM images show the tubular (a) and well-dispersed (b) features. The well-dispersed unsupported Pd−Au BHTs were obtained under ultrasound treatment after complete removal of the AAO template with NaOH (1.0 M). (c) TEM image of unsupported Pd−Au BHTs. HRTEM images of (d) a single particle, (e) overlapped Pd−Au particles near the edge of the pore area, and (f) Au−Au particle interface, respectively.

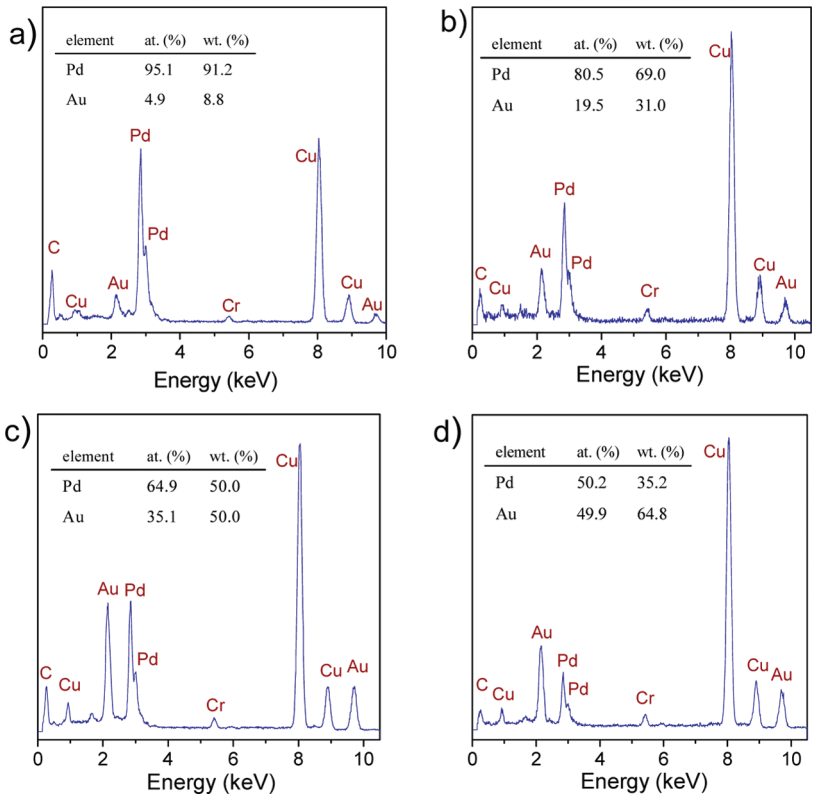

Figure 3. Representative EDX spectra of the unsupported Pd−Au BHTs prepared with different atom percentage of Pd: (a) 95.1, (b) 80.5, (c) 64.9, (d) 50.2. The measurements were performed on the surface of Pd−Au BHTs with a circular area of about 300 nm diameter.

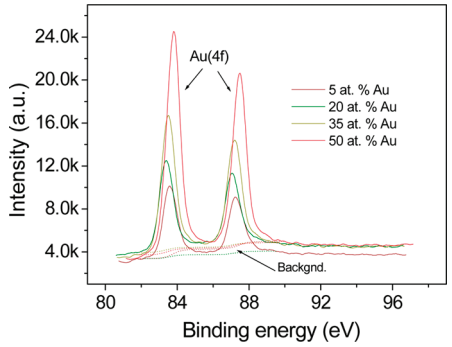

Figure 4. Au(4f) spectra of the unsupported Pd−Au BHTs with different Au atomic percentage. The surface atomic proportion of these samples can be obtained by calculating the area proportion.

were further studied through measuring the surfaces of the Pd−Au BHTs by X-ray photoelectron spectroscopy (XPS) (Figure 4). The XPS results show that the signal for Au is significantly increased by increasing the Au component.

We further characterized the resultant phase of the Pd−Au BHTs by means of powder X-ray diffraction (XRD) (see Figure 5). The reflections for the Pd−Au BHT samples appeared at 38.2° for Au and 40.1° for Pd, and these BHT materials have similar diffraction patterns with that for the physical mixture of Pd and Au particles.[22] Thereby, the two different phases seem to correspond to a separated phase with heterostructure, and interdiffusion may occur at the interface. The relative diffraction intensity of Au(111) planes increases with increasing Au atom percentage. However, Pd NPs have relatively low diffraction intensities due to the smaller particle size and relatively low crystallinity with respect to Au NPs.[18] So when the Pd was reduced to 65 atom %, the diffraction patterns of Pd NPs were overlaid. As the tube wall is constructed by plenty of overlapped tiny NPs about 3−8 nm, and the depth of field for different particle location is different, the diffraction pattern is difficult to be analyzed. So thinner wall area near a hole was selected for study. According to reported literature,[5,23−25] the Pd−Au bimetallic particles prepared by simultaneous alcohol reduction tend to form Au(core)−Pd(shell) structure due to the reduction potential difference and the accelerated reduction of $[AuCl_4]^-$ by addition of Pd^{II} as "electron-mediating". As shown in Figure 2d, the HRTEM image obtained on a single nanocrystal shows a lattice spacing of *ca.* 0.236 nm, corresponding to the Au(111) planes in the fcc Au. Within the mixing area, the particle interfaces can be easily observed (Figure 2e). The Au−Au interface is found when Au atom percentage was increased to 35% (Figure 2f). Moreover, the signal of Au(4d) was detected by XPS by increasing the Au component, which is supporting evidence for the heterostructure (Figure 6e).

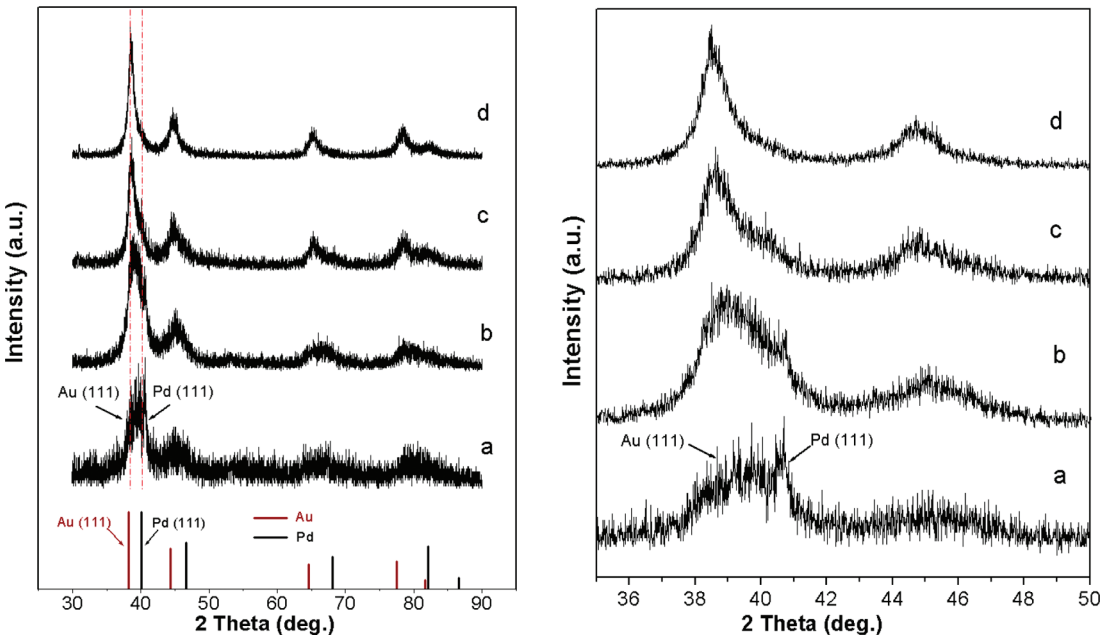

Figure 5. XRD evolution patterns of the unsupported Pd–Au BHTs by decreasing the Pd chemical composition (JCPDS no. 04-0784; JCPDS no. 46-1043): (a) 95 atom % Pd, (b) 80 atom % Pd, (c) 65 atom % Pd; (d) 50 atom % Pd.

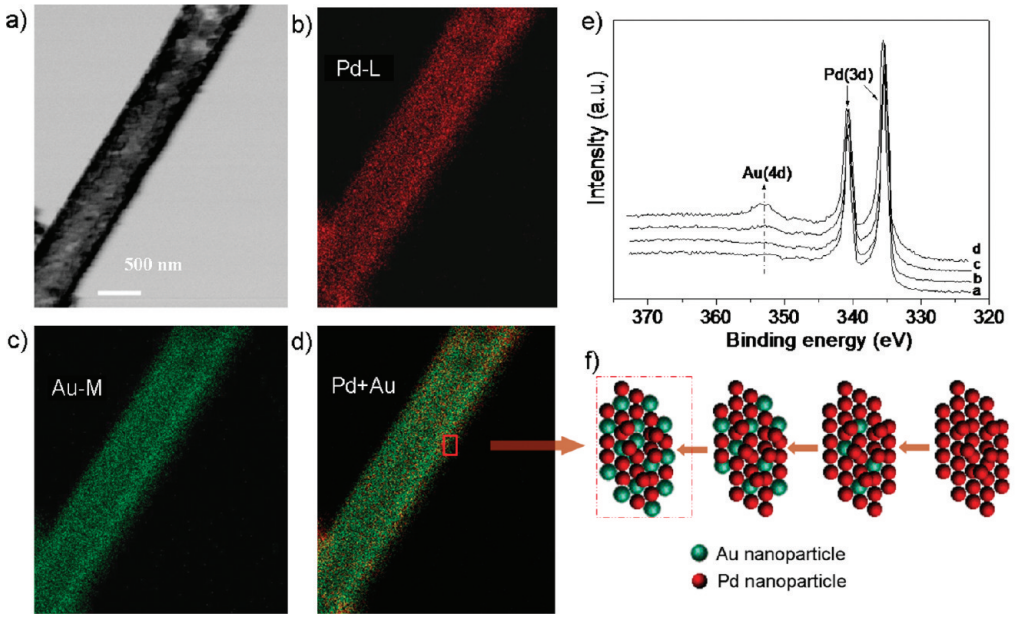

Figure 6. (a) TEM image from part of single unsupported Pd–Au BHTs (65 atom % and 50 wt %). Montage showing the corresponding EDX mappings of (b) the Pd–L and (c) Au–M signals (Pd, red; Au, green). (d) Reconstructed Pd–Au bimetallic NP submicrometer tubes. (e) Pd(3d) and Au(4d) spectra of the unsupported Pd–Au BHTs with different Pd atom percentage: (a) 95, (b) 80, (c) 65, (d) 50. (f) Simplified schematic illustration of the interface increasing with addition of the Au component. The number of Au particles increases through the addition of the Au component, and then the interface increases.

The elemental distribution of Au and Pd metals was studied by EDX mapping. Figure 6a–d shows representative scanning TEM images and the corresponding EDX mappings for Pd–Au BHTs, revealing that the elements Au and Pd are uniformly dispersed in BHTs. The elemental distribution can represent the particle distribution. The homogeneous mixtures of Pd and Au NPs can provide a large number of interfaces (Figure 6f), and these interfaces may be regarded as active sites with special electronic structure, which is a desired material for the study of interface effect on catalytic activity.

The interface effect on electrocatalytic activity was determined by investigating the catalytic activity for ethanol oxidation in alkaline solution. Figure 7a shows the cyclic voltammograms (CVs) of these catalysts including Au NP tubes, Pd NP tubes, unsupported

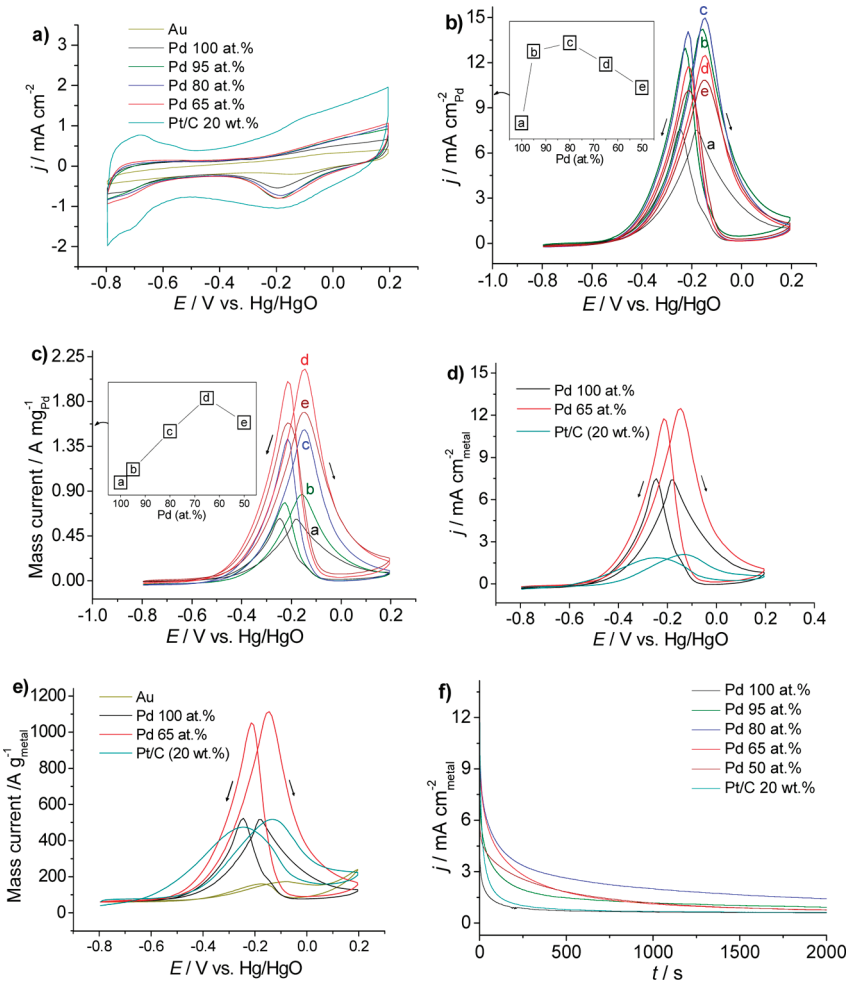

Figure 7. Cyclic voltammograms (CVs) for determining the relative ECSA change of Pd and electrocatalytic activity. (a) CVs recorded in a N_2-purged 1.0 M KOH solution at room temperature. Pseudo-area activity (b) and mass activity (c) of unsupported Pd−Au BHTs with different Pd atom percentage for ethanol oxidation in 1.0 M KOH + 1.0 M C_2H_5OH. The insets show the peak current variation by increasing the Au atom percentage. (d) Pseudo-area activity and (e) mass activity of Pd NP tubes, unsupported Pd−Au BHTs, and Pt/C catalyst. (f) Chronoamperometric curves for ethanol electro-oxidation at −0.3 V *versus* Hg/HgO on Pd NP tubes, unsupported Pd−Au BHTs, and Pt/C catalyst. Scan rate: 50 mV/s.

Pd−Au BHTs, and state-of-the-art commercial Pt/C catalyst (Johnson-Matthey, 20 wt %; for TEM images, see Figure S4) in N_2-purged 1.0 M KOH aqueous solution without ethanol at a sweep rate of 50 mV/s on newly polished glassy carbon electrode (GCE). The electrochemically active surface area (ECSA) of the catalysts can be obtained by calculating the areas of hydrogen adsorption/desorption after the deduction of the double layer region on the CV curves.[26,27] In this experiment, the Au does not participate in hydrogen adsorption/desorption, thus the hydrogen adsorption should mainly occur because of the Pd component. However, due to the absorption of hydrogen not only on Pd but also on Pd, the adsorption/desorption charge of hydrogen should be calibrated by a different potential scan rate. The relative hydrogen adsorption change of the Pd component on the backward sweep can qualitatively represent the variation of Pd relative active area. Thus the area activity, *j*, represents the activity of Pd surface sites modified by Au, named "*pseudo-area activity*". The atom and mass percentages of Pd changed from 100 to 50% and 100 to 35%, respectively, but the total mass loading is kept the same (the total metal loading is 2 μg, which is Pd *plus* Au). Initially, the catalytic activity increases with the increase of Au component and then decreases when the Au atom percentage is increased to 35% (50 wt % Au) in Figure 7b. Because the pure Au has very low catalytic activity per mass for ethanol oxidation (Figure 7e), while the relative mass of Pd was decreased sequentially, the improved catalytic activity should not be ascribed to the increase of Au mass but to the synergistic effect between Pd and Au, especially the particle interfaces. The following decrease of the catalytic activity is also attributed to the relative drop of particle interface because more than 50 wt % Au increases. Moreover, we also studied the area activity by the use of the Pd oxide reduction peak for representation of Pd ECSA.[28] It is observed that the variation trend of area activity is very similar to that based on

hydrogen adsorption calculated Pd ECSA (Supporting Information Figure S5). The results exhibited well-defined volcano-shaped activity dependence on relative Pd component. On the other hand, if the mass of Pd was constant, the catalytic activity should increase with the addition of Au due to successive increase of the interface. As shown in Figure 7c, the catalytic activity was continuously improved as desired. Although excess increase of the Au component causes the decrease of catalytic activity, which is comprehensible because Pd NPs can be somewhat isolated by Au NPs, the catalytic activity increases. Both the pseudo-area activity and the mass activity suggested the obvious improvement of the catalytic activity in the present case. This enhancement may be due to the electronic structure and local reactivity and a significant coupling of d orbitals at the Pd/Au particle interfaces.[29−31] As shown in Figure 4, XPS results show significant shifts of the Au(4f) peaks toward lower binding energies, indicating a modification of the electronic structure of the metal (ligand effect). This kind of interface interaction of Pd and Au particles, which may demonstrate similar function to those of Pt-around-Au nanocomposite by electrostatic self-assembly or a monolayer of active metal on a fine metal,[32,33] can illuminate the promotional effect of unsupported Pd−Au BHTs.

The pseudo-area activity and mass activity of the monometallic NP tube catalysts and commercial Pt/C are also studied in Figure 7d,e. Compared with the monometallic catalysts and commercial Pt/C catalyst, the unsupported Pd−Au BHTs show higher catalytic activity. The possible error of this calculated charge surface area conversion may result in an underestimation of the Pd ECSA due to the hydrogen adsorption/desorption difference between Pd and Pt and overestimation of the area activity, but combining the mass activity should provide more convincing data for the activity enhancement compared to Pt/C catalyst. For Pt/C catalyst in alkaline media, the higher hydroxyl adsorption on Pt and the formation of CO-like intermediates during the oxidation of alcohol may inhibit the activity of Pt.[2,13] When the atom percentage of Pd is up to 65%, the mass activity increases to more than 1000 $A/g_{(Pd+Au)}$, which is 3 times greater than the mass activity of the unsupported Pd nanowire arrays.[34] The results indicate that the unsupported Pd−Au BHTs can be used as catalysts in direct alcohol fuel cells (DAFCs).

To evaluate the long-term electrocatalytic performance, the chronoamperograms of the unsupported Pd−Au BHTs and commercial Pt/C catalyst were recorded with a bias at −0.3 V *versus* Hg/HgO in 1.0 M KOH + 1.0 M C_2H_5OH at room temperature (Figure 7f). It is observed that the ethanol oxidation current of Pd−Au BHTs initially increases with decreasing Pd component ratio and then sharply decays within 0 and 500 s at less than 80 atom % Pd. In alkaline media, C−C bond breaking is more facile and then rapidly converted to CO_{ad} upon adsorption.[35] This degradation may be due to a mass of intermediate species adsorbed on the highly active Pd/Au interface sites and then blocked the further reactivity. After all, the mass activity of Pd already reached the maximum values (Figure 7c). However, the rational reasons for such a phenomenon are not clear at this stage. At the end of the 2000 s test, the oxidation current on the Pd−Au BHTs (80 atom % Pd) is considerably higher than other Pd component ratios and Pt/C catalyst, indicating a high electrocatalytic activity and stability around this ratio.

In conclusion, the present study describes an unsupported Pd−Au bimetallic heterostructure submicrometer tubular nanostructure for studying the synergistic effect of interface on electrocatalytic activity. The interface of this bimetallic system can be finely controlled by tuning the chemical composition of Pd and Au through the one-step non-aqueous solvent electrodeposition method and then adjusting the proportion of Pd and Au NPs which are homogeneously distributed in tubes. As-synthesized unique unsupported Pd−Au BHTs display remarkably enhanced catalytic activity over those of the monometallic catalysts or even commercial Pt/C catalyst, representing that they can act as efficient Pt-free catalysts for fuel cells or other applications.

METHODS

Chemicals. $NaNO_3$, $PdCl_2$, $AuCl_3 \cdot HCl \cdot 4H_2O$, dimethyl sulfoxide (99% w/w), C_2H_5OH (≥99.7% w/w), KOH, and NaOH were commercially available from Shanghai Chemical Reagent Co. Ltd. and Nafion (5 wt %) from Sigma-Aldrich. All chemical reagents were analytical grade and used as received without further purification.

Electrochemical Synthesis of Unsupported Pd−Au BHTs. The commercial anodic aluminum oxide (AAO) template (Anodisc 47, Whatman Co., UK) with the channel diameter of about 300 nm by SEM sputtered with thin Au layer on one side about 40 nm thick to form an annular base electrode at the bottom of the nanopores. This thin Au layer was used as working electrode in the subsequent electrodeposition of the desired Pd−Au BHTs. The experiments were performed potentiostatically at −1.3 to −1.6 V *vs* Ag/AgCl (3 M) in anhydrous DMSO solvents mixed with 10 mM $PdCl_2$ and different concentrations of $AuCl_3 \cdot HCl \cdot 4H_2O$ (Figure 1); 100 mM $NaNO_3$ was added in all of the reactions for supporting electrolyte. The counter electrode is Pt foil. After electrodeposition, the thin Au layer on one side of the AAO template was erased completely by alumina particles, and then the Pd−Au BHTs were exposed by immerging in 1.0 M NaOH solution for 1 h to completely remove the AAO, followed by washing with doubly deionized H_2O and ethanol several times.

Electrocatalytic Study. The electrochemical catalytic activity of the unsupported Pd–Au BHTs was investigated using a three-electrode system on an IM6ex electrochemical workstation (Zahner, Germany). A platinum foil (1.0 cm^2) and Hg/HgO (1.0 M KOH) were used as the counter and reference electrodes, respectively. A glassy carbon electrode (GCE, 3 mm diameter, 0.07 cm^2) served as substrate for the supported catalyst and was polished to a mirror finish (No. 40-6365-006, Gamma Micropolish Alumina, Buehler; No.40-7212, Microcloth, Buehler) and thoroughly cleaned. GCE that was used as support in this experiment has negligible effect on the catalytic study. For the preparation of the catalytic electrode, ethanol suspensions of 1 mg mL^{-1} catalyst with 0.02 wt % Nafion (diluted from 5 wt % Nafion, Sigma-Aldrich) were obtained by ultrasonic mixing for about 20 min. Two micrograms of catalyst was transferred onto the GCE substrate, leading to the low metal loading of 28.31 $\mu g/cm^2$ for Au NP tubes, unsupported Pd–Au BHTs, and Pt/C catalyst. Finally, the as-prepared catalyst GCE was dried for 1 h in air at room temperature. Cyclic voltammetric curves were obtained at a scan rate of 50 mV s^{-1} at room temperature with the potential range of −0.8 to 0.2 V *versus* Hg/HgO. The electrochemical surface areas were calculated from hydrogen desorption peak of the CV cycles in N_2-purged 1.0 M KOH solution. The catalytic activity was measured in 1.0 M KOH + 1.0 M C_2H_5OH solutions.

Characterization. The resultant phase of the as-synthesized Pd–Au BHTs was examined by XRD (Cu K radiation, 0.154056 nm). SEM images were obtained with a Zeis SupraTM 40 high-resolution field emission scanning electron microscope operating at 5 kV. Energy-dispersive X-ray spectra (EDX) were taken with a JEOJ-2010 transmission electron microscope with an acceleration voltage of 200 kV. TEM and HRTEM images were obtained using JEOJ-2010 TEM. The wide views of TEM images were achieved by an H-7650 transmission electron microscope. X-ray photoemission spectrometry image was recorded on ESCALAB-MK-II. Inductively coupled plasma mass (ICP) data were obtained by Optima 7300 DV.

Acknowledgment. S.H.Y. acknowledges the funding support from the National Basic Research Program of China (2010CB934700), the National Natural Science Foundation of China (Nos. 91022032, 50732006), and International Science & Technology Cooperation Program of China (2010DFA41170).

Supporting Information Available: SEM, TEM, and electrochemical characterization procedures. This material is available free of charge *via* the Internet at http://pubs.acs.org.

REFERENCES AND NOTES

1. Chen, M.; Kumar, D.; Yi, C.-W.; Goodman, D. W. The Promotional Effect of Gold in Catalysis by Palladium–Gold. *Science* **2005**, *310*, 291–293.
2. Bianchini, C.; Shen, P. K. Palladium-Based Electrocatalysts for Alcohol Oxidation in Half Cells and in Direct Alcohol Fuel Cells. *Chem. Rev.* **2009**, *109*, 4183–4206.
3. Bell, A. T. The Impact of Nanoscience on Heterogeneous Catalysis. *Science* **2003**, *299*, 1688–1691.
4. Lim, B.; Jiang, M.; Camargo, P. H. C.; Cho, E. C.; Tao, J.; Lu, X.; Zhu, Y.; Xia, Y. Pd–Pt Bimetallic Nanodendrites with High Activity for Oxygen Reduction. *Science* **2009**, *324*, 1302–1305.
5. Lee, H. J.; Habas, S. E.; Somorjai, G. A.; Yang, P. D. Localized Pd Overgrowth on Cubic Pt Nanocrystals for Enhanced Electrocatalytic Oxidation of Formic Acid. *J. Am. Chem. Soc.* **2008**, *130*, 5406–5407.
6. Ksar, F. a.; Ramos, L.; Keita, B.; Nadjo, L.; Beaunier, P.; Remita, H. Bimetallic Palladium–Gold Nanostructures: Application in Ethanol Oxidation. *Chem. Mater.* **2009**, *21*, 3677–3683.
7. Guo, Y. G.; Hu, J. S.; Zhang, H. M.; Liang, H. P.; Wan, L. J.; Bai, C. L. Tin/Platinum Bimetallic Nanotube Array and Its Electrocatalytic Activity for Methanol Oxidation. *Adv. Mater.* **2005**, *17*, 746–750.
8. Zhao, D.; Xu, B.-Q. Enhancement of Pt Utilization in Electrocatalysts by Using Gold Nanoparticles. *Angew. Chem., Int. Ed.* **2006**, *45*, 4955–4959.
9. Kwak, J. H.; Hu, J.; Mei, D.; Yi, C.-W.; Kim, D. H.; Peden, C. H. F.; Allard, L. F.; Szanyi, J. Coordinatively Unsaturated Al^{3+} Centers as Binding Sites for Active Catalyst Phases of Platinum on γ-Al_2O_3. *Science* **2009**, *325*, 1670–1673.
10. Valden, M.; Lai, X.; Goodman, D. W. Onset of Catalytic Activity of Gold Clusters on Titania with the Appearance of Nonmetallic Properties. *Science* **1998**, *281*, 1647–1650.
11. Matthey, D.; Wang, J. G.; Wendt, S.; Matthiesen, J.; Schaub, R.; Laegsgaard, E.; Hammer, B.; Besenbacher, F. Enhanced Bonding of Gold Nanoparticles on Oxidized TiO_2(110). *Science* **2007**, *315*, 1692–1696.
12. Herzing, A. A.; Kiely, C. J.; Carley, A. F.; Landon, P.; Hutchings, G. J. Identification of Active Gold Nanoclusters on Iron Oxide Supports for CO Oxidation. *Science* **2008**, *321*, 1331–1335.
13. Zheng, H. T.; Li, Y. L.; Chen, S. X.; Shen, P. K. Effect of Support on the Activity of Pd Electrocatalyst for Ethanol Oxidation. *J. Power Sources* **2006**, *163*, 371–375.
14. Yang, Y.; Saoud, K. M.; Abdelsayed, V.; Glaspell, G.; Deevi, S.; El-Shall, M. S. Vapor Phase Synthesis of Supported Pd, Au, and Unsupported Bimetallic Nanoparticle Catalysts for CO Oxidation. *Catal. Commun.* **2006**, *7*, 281–284.
15. Spendelow, J. S.; Wieckowski, A. Electrocatalysis of Oxygen Reduction and Small Alcohol Oxidation in Alkaline Media. *Phys. Chem. Chem. Phys.* **2007**, *9*, 2654–2675.
16. Nie, M.; Tang, H.; Wei, Z.; Jiang, S. P.; Shen, P. K. Highly Efficient AuPd-WC/C Electrocatalyst for Ethanol Oxidation. *Electrochem. Commun.* **2007**, *9*, 2375–2379.
17. Cui, C. H.; Li, H. H.; Yu, J. W.; Gao, M. R.; Yu, S. H. Ternary Heterostructured Nanoparticle Tubes: A Dual Catalyst and Its Synergistic Enhancement Effects for O_2/H_2O_2 Reduction. *Angew. Chem., Int. Ed.* **2010**, *49*, 9149–9152.
18. Cui, C. H.; Li, H. H.; Yu, S. H. A General Approach to Electrochemical Deposition of High Quality Free-Standing Noble Metal (Pd, Pt, Au, Ag) Sub-Micron Tubes Composed of Nanoparticles in Polar Aprotic Solvent. *Chem. Commun.* **2010**, *46*, 940–942.
19. Chen, Z. W.; Waje, M.; Li, W. Z.; Yan, Y. S. Supportless Pt and PtPd Nanotubes as Electrocatalysts for Oxygen-Reduction Reactions. *Angew. Chem., Int. Ed.* **2007**, *46*, 4060–4063.
20. Eftekhari, A. *Nanostructured Materials in Electrochemistry*; Wiley-VCH: Weinheim, Germany, 2008.
21. Izutsu, K. *Electrochemistry in Nonaqueous Solutions*, Wiley-VCH: Weinheim, Germany, 2009.
22. Wu, M.-L.; Chen, D.-H.; Huang, T.-C. Synthesis of Au/Pd Bimetallic Nanoparticles in Reverse Micelles. *Langmuir* **2001**, *17*, 3877–3883.
23. Alayoglu, S.; Nilekar, A. U.; Mavrikakis, M.; Eichhorn, B. Ru–Pt Core–Shell Nanoparticles for Preferential Oxidation of Carbon Monoxide in Hydrogen. *Nat. Mater.* **2008**, *7*, 333–338.
24. Luo, J.; Wang, L.; Mott, D.; Njoki, P. N.; Lin, Y.; He, T.; Xu, Z.; Wanjana, B. N.; Lim, I.-I. S.; Zhong, C.-J. Core/Shell Nanoparticles as Electrocatalysts for Fuel Cell Reactions. *Adv. Mater.* **2008**, *20*, 4342–4347.
25. Toshima, N.; Yonezawa, T. Bimetallic Nanoparticles: Novel Materials for Chemical and Physical Applications. *New J. Chem.* **1998**, *22*, 1179–1201.
26. Correia, A. N.; Mascaro, L. H.; Machado, S. A. S.; Avaca, L. A. Active Surface Area Determination of Pd–Si Alloys by H-Adsorption. *Electrochim. Acta* **1997**, *42*, 493–495.
27. Schmidt, T. J.; Gasteiger, H. A.; Stab, G. D.; Urban, P. M.; Kolb, D. M.; Behm, R. J. Characterization of High-Surface Area Electrocatalysts Using a Rotating Disk Electrode Configuration. *J. Electrochem. Soc.* **1998**, *145*, 2354–2358.
28. Xiao, L.; Zhuang, L.; Liu, Y.; Lu, J. T.; Abruna, H. D. Activating Pd by Morphology Tailoring for Oxygen Reduction. *J. Am. Chem. Soc.* **2009**, *131*, 602–608.
29. Taguchi, N.; Tanaka, S.; Akita, T.; Kohyama, M.; Hori, F. First-Principles Calculations of the Atomic and Electronic Structures in Au–Pd Slab Interfaces. *Solid State Phenom.* **2008**, *139*, 29–33.
30. Tanaka, S.; Taguchi, N.; Akita, T.; Hori, F.; Kohyama, M. First-Principles Calculations of Pd/Au(100) Interfaces with Adsorbates. *Solid State Phenom.* **2008**, *139*, 47–52.
31. Roudgar, A.; Gross, A. Local Reactivity of Supported Metal Clusters: Pd_n on Au(111). *Surf. Sci.* **2004**, *559*, L180–L186.

32. Zhang, S.; Shao, Y.; Yin, G.; Lin, Y. Electrostatic Self-Assembly of a Pt-Around-Au Nanocomposite with High Activity towards Formic Acid Oxidation. *Angew. Chem., Int. Ed.* **2010**, *49*, 2211–2214.
33. Adzic, R. R.; Zhang, J.; Sasaki, K.; Vukmirovic, M. B.; Shao, M.; Wang, J. X.; Nilekar, A. U.; Mavrikakis, M.; Valerio, J. A.; Uribe, F. Platinum Monolayer Fuel Cell Eectrocatalysts. *Top. Catal.* **2007**, *46*, 249–262.
34. Xu, C. W.; Wang, H.; Shen, P. K.; Jiang, S. P. Highly Ordered Pd Nanowire Arrays as Effective Electrocatalysts for Ethanol Oxidation in Direct Alcohol Fuel Cells. *Adv. Mater.* **2007**, *19*, 4256–4259.
35. Lai, S. C. S.; Kleijn, S. E. F.; Öztürk, F. T. Z.; van Rees Vellinga, V. C.; Koning, J.; Rodriguez, P.; Koper, M. T. M. Effects of Electrolyte pH and Composition on the Ethanol Electrooxidation Reaction. *Catal. Today* **2010**, *154*, 92–104.